RESEARCH Open Access



Bystander neuronal progenitors in forebrain organoids promote protective antiviral responses

Seble G. Negatu¹, Christine Vazquez^{1†}, Carl Bannerman^{1†}, Kevin R. Amses¹, Guo-Li Ming² and Kellie A. Jurado^{1*}

Abstract

Neurotropic viruses are the most common cause of infectious encephalitis and highly target neurons for infection. Our understanding of the intrinsic capacity of neuronal innate immune responses to mediate protective antiviral responses remains incomplete. Here, we evaluated the role of intercellular crosstalk in mediating intrinsic neuronal immunity and its contribution to limiting viral infection. We found that in the absence of viral antagonism, neurons transcriptionally induce robust interferon signaling and can effectively signal to uninfected bystander neurons. Yet, in two-dimensional cultures, this dynamic response did not restrict viral spread. Interestingly, this differed in the context of viral infection in three-dimensional forebrain organoids with complex neuronal subtypes and cellular organization, where we observed protective capacity. We showed antiviral crosstalk between infected neurons and bystander neural progenitors is mediated by type I interferon signaling. Using spatial transcriptomics, we then uncovered regions containing bystander neural progenitors that expressed distinct antiviral genes, revealing critical underpinnings of protective antiviral responses among neuronal subtypes. These findings underscore the importance of interneuronal communication in protective antiviral immunity in the brain and implicate key contributions to protective antiviral signaling.

Introduction

The brain houses a mosaic of molecularly distinct cellular subtypes that form complex intercellular networks. Neurotropic viruses target the brain for infection, often with a preference for replication within neurons [1, 2]. Although neurons express pattern recognition receptors that allow them to sense viruses and activate innate

[†]Christine Vazquez and Carl Bannerman contributed equally.

Kellie A. Jurado: Lead contact.

*Correspondence: Kellie A. Jurado

kellie.jurado@pennmedicine.upenn.edu

immune pathways [3], neurons are still considered passive targets during viral infection while resident glia cells are considered to be the primary cells that coordinate antiviral immunity [4]. Molecular cross-talk between glial cells and neurons has been proposed to facilitate immune activation in neighboring glia [4]. Whether these mechanisms also allow for cross-talk among neuronal subtypes and enable neurons to contribute to overall antiviral immunity has not been explored.

The type I interferon (IFN) response is the primary driver of an antiviral state in many cells. Neurons have been reported as IFN-producing cells upon infection with neurotropic viruses [5, 6]. Moreover, neurons have a capacity to elicit innate immune signatures; albeit, neuronal subtypes have differential innate immune capacities that are influenced by regionality or maturation state [7–9]. Together, this supports that neurons have potential



© The Author(s) 2025. **Open Access** This article is licensed under a Creative Commons Attribution-NonCommercial-NoDerivatives 4.0 International License, which permits any non-commercial use, sharing, distribution and reproduction in any medium or format, as long as you give appropriate credit to the original author(s) and the source, provide a link to the Creative Commons licence, and indicate if you modified the licensed material. You do not have permission under this licence to share adapted material derived from this article or parts of it. The images or other third party material in this article are included in the article's Creative Commons licence, unless indicated otherwise in a credit line to the material. If material is not included in the article's Creative Commons licence and your intended use is not permitted by statutory regulation or exceeds the permitted use, you will need to obtain permission directly from the copyright holder. To view a copy of this licence, visit http://creativecommons.org/licenses/by-nc-nd/4.0/.

¹ Department of Microbiology, University of Pennsylvania Perelman School of Medicine, Philadelphia, PA, USA

² Department of Neuroscience, University of Pennsylvania Perelman School of Medicine, Philadelphia, PA, USA

to be important contributors to an antiviral state during neurotropic infections.

Many viruses have evolved to antagonize type I IFN signaling to evade activation of innate immune responses. For example, La Crosse virus (LACV) is a neuron-targeting RNA virus that is the primary cause of pediatric encephalitis in the United States, which has a non-structural protein in its S segment (NSs) that blunts antiviral IFN responses [10, 11]. Studies suggest neurotropic viruses ability to suppress antiviral pathways promotes viral persistence in neurons [4]. This viral antagonism occurs only in infected cells, making immune signaling in uninfected bystander cells essential for limiting viral spread [12]. How uninfected bystander neurons contribute to the overall coordinated antiviral response in the central nervous system remains unexplored.

This gap led us to investigate the role of intercellular crosstalk between infected neurons and uninfected bystanders in mediating intrinsic neuronal immunity and its contribution to protective antiviral responses. We demonstrate that neurons have a strong ability to sense viral infection and elicit robust innate immune signatures when viral antagonism is limited. Using a forebrain organoid model with complex neuronal subtypes and organization, we reveal antiviral crosstalk between infected neurons and bystander neural progenitors that is mediated by type I IFN signaling. Using spatial transcriptomics, we then uncover distinct regions containing bystander neural progenitors and reveal underpinnings of protective antiviral responses in neurons. These findings underscore the importance of intercellular communication among neuronal subtypes in protective antiviral immunity in the brain and implicate key contributions to protective antiviral signaling.

Results

Viral antagonism masks neuronal intrinsic capacity to induce robust interferon signaling.

Neurons have long been considered poor IFN producers [5–7, 13–15]; however, neuronal potential to mount effective IFN responses to viral infection has been primarily modeled using viruses that antagonize innate immune activation [16]. Thereby, we first evaluated if neurons had increased capacity to intrinsically induce antiviral pathways in the absence of immune antagonism. We cultured embryonic murine cortical neurons for 9-days prior to infection with WT-LACV or ΔNSs-LACV, a strain that lacks the well-defined viral antagonist NSs (ΔNSs-LACV mutant validation in Supplemental Figs. 1A and 1B) [11, 17]. Mechanistically, LACV NSs and cofactor Elongin C (an E3 ubiquitin ligase) target RPB1 proteins within elongating RNA polymerase II complexes for degradation, thereby suppressing global mRNA synthesis [18].

Additionally, given previous reports that neurons have functional and intact PRR pathway activity [3], we sought to determine gene expression changes upon extracellular neuronal exposure to LACV PAMPs by exposing cultures to heat- or UV-inactivated $\Delta NSs\text{-LACV}$. To define neuronal innate immune potential in an unbiased manner, we conducted bulk RNA sequencing at 16-h post-infection (HPI) (Fig. 1A). WT- and $\Delta NS\text{-LACV}$ -infected neurons formed distinct clusters on a PCA plot, indicating they had unique responses to infection (Fig. 1B). In contrast, neuronal cultures treated with heat- or UV-inactivated $\Delta NS\text{-LACV}$ largely clustered with mock, signifying viral replication drives robust changes in neuronal gene expression.

Unbiased clustering of 4057 differentially expressed genes revealed 6 unique clusters (Fig. 1C). Cluster 5 represented genes upregulated in both WT- or ΔNSs -LACV-infected neurons but more highly induced with WT-LACV infection. Pathway analysis of these genes uncovered activation of inflammatory pathways such as NF-κB signaling and production of cytokines including tumor necrosis factor (Fig. 1D). In contrast, cluster 6 denoted genes that were uniquely upregulated in the ΔNSs-LACV-infected samples. Regulation of transcription by RNA polymerase II was upregulated in ΔNSs-LACV-infected samples, corroborating that the NSs protein antagonizes host gene expression by limiting RNA polymerase II function (Fig. 1E). Interestingly, functional enrichment analysis showed specific induction of viral recognition machinery such as RIG-I signaling and the type I IFN antiviral pathway in the absence of viral antagonism. To evaluate drivers of this specificity in ΔNSs-LACV-infected neurons, we gueried representative innate antiviral genes in cluster 6. We observed increased gene expression of upstream signaling mediators such as Ifnb and downstream IFN-stimulated genes (ISGs) including Ifit1 and Ifit3 in ΔNSs-LACV-infected neurons compared to WT-LACV (Fig. 1F). These differences were not attributable to viral PAMPs as WT- and ΔNSs-LACV had similar viral RNA levels (Fig. 1G). These data suggest that in the absence of viral antagonism, primary murine cortical neurons have a strong capacity to sense pathogens and induce expression of IFN-specific genes.

Uninfected bystander neurons induce innate immune responses.

Given that ΔNSs-LACV infection of murine neurons distinctly elicited robust IFN signaling, we used it to investigate whether the observed antiviral responses were unique to infected neurons or nearby uninfected bystander neurons. We utilized validated LACV-targeting fluorescence in-situ hybridization (FISH) probes

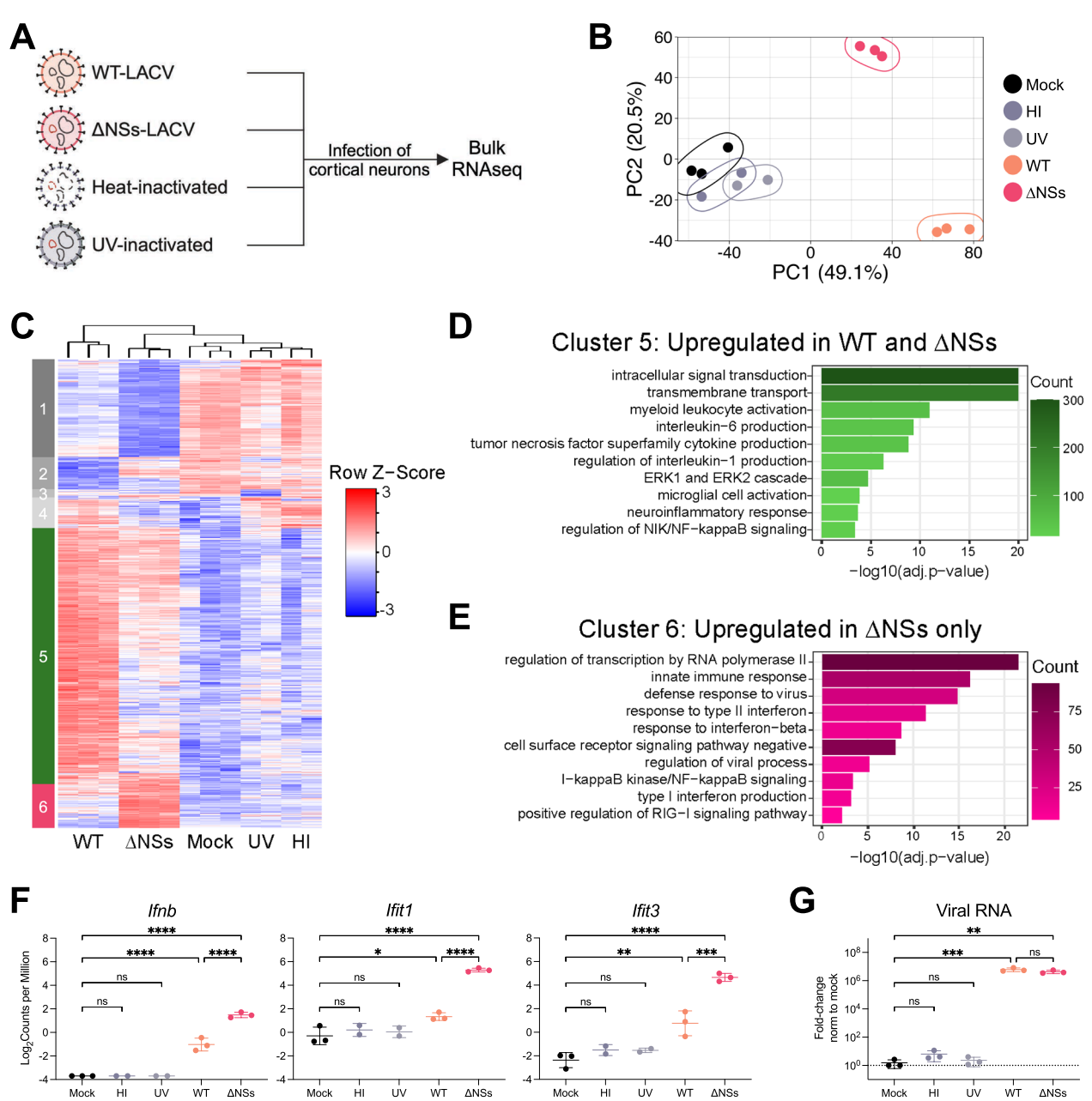


Fig. 1 Viral antagonism masks neuronal intrinsic capacity to induce robust interferon signaling. Primary cortical neurons were isolated from murine embryo cortices at embryonic day 16.5. Isolated neurons were either mock-treated (Mock) or infected at 0.5 MOI for 16 h with wild-type-La Crosse Virus (WT-LACV); recombinant ΔNSs-La Crosse Virus (ΔNSs-LACV); heat-inactivated ΔNSs-LACV (HI); or ultraviolet-inactivated ΔNSs-LACV (UV) followed by bulk RNA sequencing of total RNA. **A** Schematic of experimental design. **B** Principal component analysis showing PC1 and PC2 for bulk RNA sequencing data from mock-treated and infected neurons. **C** Heat map of gene expression data scaled by z-score for each row. Columns represent samples clustered using Spearman correlation, and rows represent differentially expressed genes compared to mock clustered using Pearson correlation. Genes in the heatmap met cutoffs of *p*-value = 0.01 and log fold-change = ±1. Functional enrichment analysis of genes from cluster 5 (**D**) and cluster 6 (**E**) using Gene Ontology biological processes. **F** Log2 adjusted counts per million of select innate antiviral genes in cluster 6. Data are presented as means ± SD. Statistical analysis performed with one-way ANOVA followed by Tukey's test. **G** Fold change of LACV RNA was determined by quantitative RT-PCR relative to the housekeeping gene *Hprt*, normalized to mock. Neurons were pooled from 2 litters. Data are presented as means ± SD. Statistical analysis performed with one-way ANOVA followed by Tukey's test, ns *p* > 0.05, **p* < 0.05, ***p* < 0.01, *****p* < 0.001, and ******p* < 0.0001

(Supplemental Fig. 1C) to demarcate $\Delta NSs\text{-}LACV$ -infected neurons prior to fluorescence-activated cell sorting (FACS) for bulk RNA sequencing (Fig. 2A) [19, 20]. We used mock-treated neurons as a threshold to define uninfected bystander cells within infected cultures and recognize low levels of the viral RNA may still be present in the bystander population. Moreover, positive LACV FISH signal was used to identify highly infected

neurons. The remaining cells were deemed an intermediately infected population. To identify a timepoint where both uninfected bystander and highly infected populations are distinguishable, neurons from infected cultures were collected at 1-, 16- and 24-HPI for FISH staining followed by flow cytometry (Fig. 2B). Quantification of the bystander, intermediate and highly infected neurons revealed a shift from majority bystanders at 1-HPI to

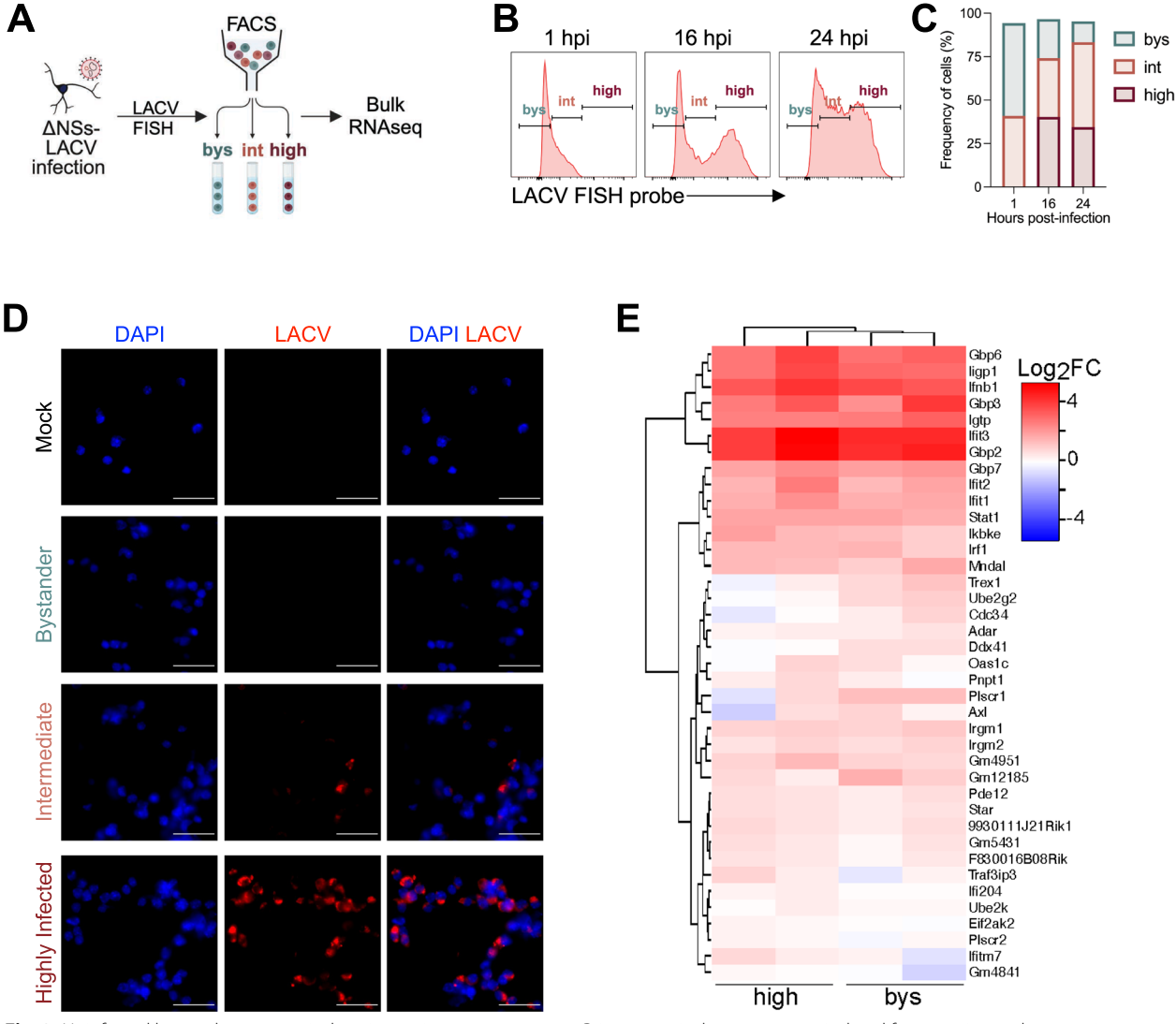


Fig. 2 Uninfected bystander neurons induce innate immune responses. Primary cortical neurons were isolated from murine embryo cortices at embryonic day 16.5. Isolated neurons were either mock-treated (Mock) or infected at 0.5 MOI for 16 h with recombinant ΔNSs-La Crosse Virus (ΔNSs-LACV). **A** Schematic of adapted probe-seq pipeline where mock-treated or ΔNSs-LACV-infected murine cortical neurons were stained with LACV FISH probes prior to FACS sorting of three populations, bystander (bys); intermediate (int); and highly infected (high) neurons, for bulk RNA sequencing. Flow cytometry analysis of ΔNSs-LACV-infected neurons stained with LACV FISH probes and collected at 1-, 16- and 24-h post-infection (HPI). Gating (**B**) and quantification (**C**) of neurons. Neurons were pooled from 1 litter. **D** Representative fluorescence images of FACS-sorted ΔNSs-LACV-infected neurons at 16-HPI. LACV RNA was labeled by FISH probes (*red*) and neurons were stained for DAPI (nuclei, *blue*). *Scale bars*—25 μm. **E** Heatmap represents the log₂ fold-change of genes from a response to interferon alpha/beta gene list in highly-infected (high) and bystander (bys) neurons relative to mock-treated cells. The gene list was curated from MSigDB GoBP's "Response to interferon alpha" and "Response to interferon beta." Neurons were pooled from 1 litter per independent experiment (N=two independent experiments)

highly infected neurons by 24-HPI (Fig. 2C). At 16-HPI we observed a bimodal distribution enabling clear separation of bystander and highly infected neurons. To validate sorting at this timepoint, we FACS-sorted ΔNSs-LACV-infected neurons at 16-HPI (gates shown in Supplemental Fig. 1D) and visualized LACV FISH signal using fluorescence microscopy (Fig. 2D). As suggested by the bimodal distribution of bystander and highly infected neurons seen by flow cytometry, uninfected bystanders lacked FISH signal, similar to mock, while highly infected neurons were all positive. However, neurons in the intermediate population had a mixed positive and negative LACV FISH signal, leading us to omit this group from further analysis.

For sequencing analysis, RNA was extracted from sorted uninfected mock, uninfected bystander and infected populations. Given the specific innate antiviral gene signature we observed in ΔNSs-LACV-infected neurons (Fig. 1E), we sought to compare the expression of type I IFN response genes between uninfected bystander and infected populations. Expression of genes selected from curated datasets of the IFN alpha/beta response pathway were evaluated (Fig. 2E). Surprisingly, unsupervised clustering revealed similar ISG expression patterns by both bystander and highly infected neurons, with the *Ifit* family of genes having elevated expression.

Taken together, these data show that during $\Delta NSs-LACV$ infection of neurons, uninfected bystanders that neighbor infected cells contribute to the robust type I IFN transcriptional signature observed. However, despite these differences, both WT and $\Delta NSs-LACV$ exhibited nearly identical growth curves (Supplemental Figs. 1D and 1E), indicating that the transcriptional induction of ISGs during $\Delta NSs-LACV$ infection does not limit viral replication or virion production in this model system.

Interneuronal communication within human forebrain organoids reveal protective ISG production by bystander neural progenitors

Murine two-dimensional cortical neuron cultures contain homogenous neuronal populations that are organized in monolayers, lacking features found in the brain that may contribute to protective antiviral responses. Therefore, we employed human induced pluripotent stem cell (iPSC)-derived forebrain organoids which mimic cortical layers of the developing human brain and contain neurons of various differentiation states [21], thus allowing interneuronal communication between progenitor and mature neurons. This three-dimensional architecture and heterogeneity of neuronal differentiation states leverages our ability to assess complex intercellular communication among neuronal subtypes that contribute to innate immune responses.

To first model the radial organization of progenitors, we generated 35-days in-vitro (DIV) forebrain organoids, which contain neural progenitor regions demarcated by SOX2 expression and are commonly referred to as neural rosettes (Supplemental Figs. 2A and 2B). Outside of these regions, MAP2 expression was observed indicating the presence of mature neurons (Supplemental Fig. 2C). Further, viability of organoids was determined by minimal TUNEL staining (Supplemental Fig. 2C). We then infected 35-DIV forebrain organoids with WT- or ΔNSs-LACV for 24 h and collected samples at 4-days post-infection (DPI) (Fig. 3A). At 4-DPI, we saw significantly less viral RNA during ΔNSs-LACV infection as compared with WT-LACV (Fig. 3B). Furthermore, IFIT1 gene expression was significantly lower in mock-treated organoids as compared with WT-LACV (Fig. 3C). While IFIT1 trended higher in ΔNSs-LACV-infected forebrain organoids compared to those infected with WT-LACV, this was not statistically significant (Fig. 3C). We also observed similar trends with MX1 and OAS2 gene expression (Supplemental Fig. 3). Together, this suggests the potential of forebrain organoids to elicit an effective antiviral response in the absence of immune antagonism.

To visualize virus localization and IFIT1 protein expression in the absence of viral antagonism, we collected \(\Delta NSs-LACV-infected \) forebrain organoids for immunofluorescence at 4-DPI (Fig. 3D). We detected substantial viral antigen throughout the periphery of the organoids. Interestingly, IFIT1 expression radiated from neural rosettes (white arrows in Fig. 3D), regions which lacked LACV signal, suggesting that ISGs were derived from bystander neurons. Given the radial IFIT1 expression pattern, we sought to further characterize IFIT1+ cells by staining ΔNSs-LACV-infected (Fig. 3E) and mock-treated organoids (Fig. 3F) for SOX2 expression, a neural progenitor marker. We observed colocalization of IFIT1 expression and SOX2 within and outside of neural rosettes (Fig. 3E). However, despite the presence of SOX2+ neural progenitors, mock-treated organoids lacked basal IFIT1 protein expression (Fig. 3F), suggesting a viral-driven IFIT1 induction.

Overall, we found that human forebrain organoids can serve as a model for neuronal-intrinsic antiviral responses. Specifically, we observed that uninfected bystander neurons inducing innate signaling that limited viral replication were neural progenitors, suggestive that bystander neural progenitors play a role in antiviral protection.

Interferon signaling within bystander neural progenitors limits viral spread and replication

We next sought to investigate the mechanism by which bystander neural progenitors contribute to the antiviral

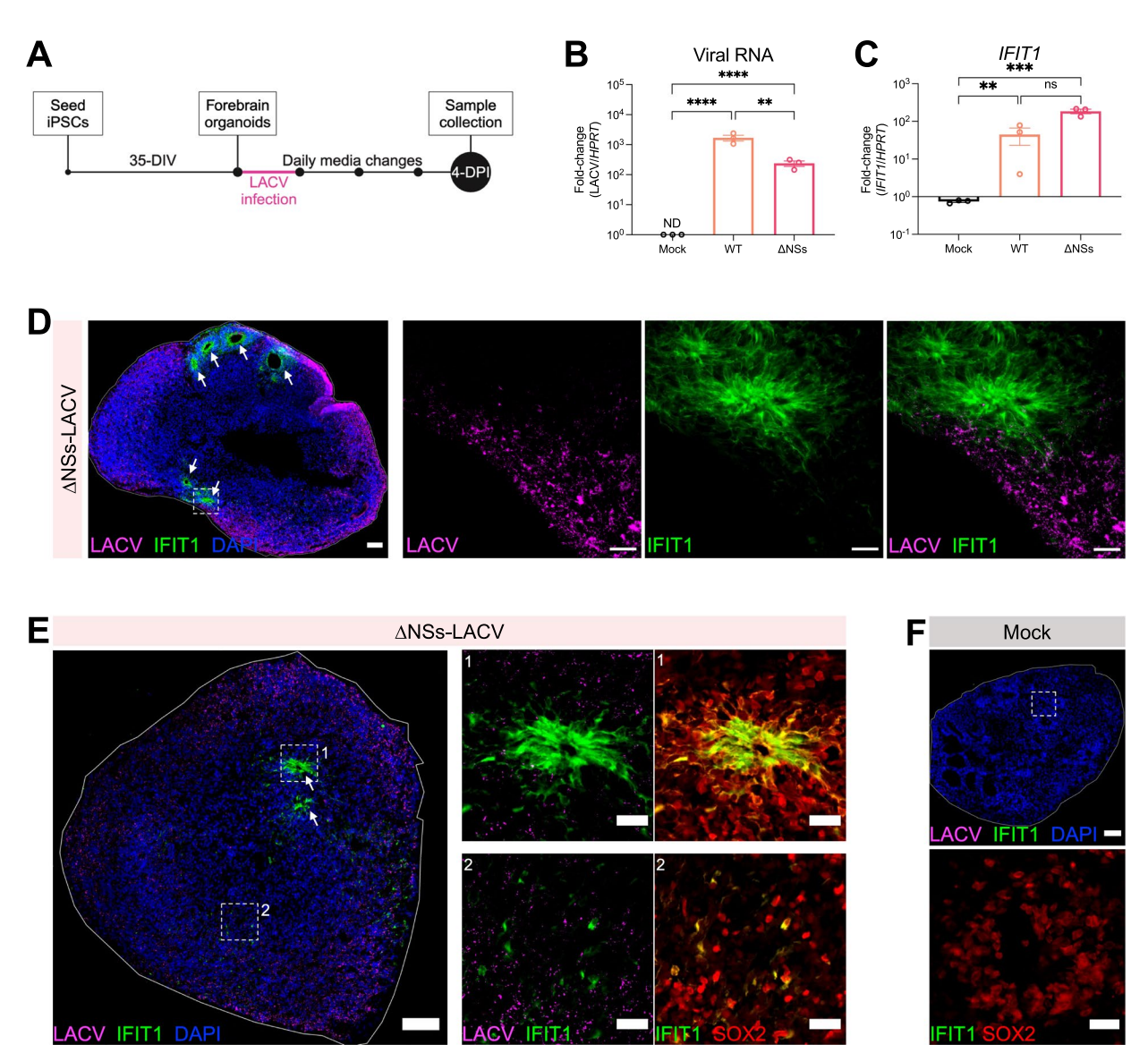


Fig. 3 Interneuronal communication within human forebrain organoids reveal protective ISG production by bystander neural progenitors. 35-days *in-vitro* (DIV) human induced pluripotent stem cell-derived forebrain organoids were infected with 2.5×10^6 PFU WT-LACV; ΔNSs-LACV; or mock treated for 24-h. Organoid media was replenished with fresh media daily until sample collection at 4-days post-infection (DPI). **A** Schematic of experimental design. Fold change of LACV RNA (**B**) and *IFIT1* (**C**) was determined by quantitative RT-PCR relative to the housekeeping gene *HPRT*. Data are presented as means ± SEM (N=three biological replicates). Statistical analysis performed with one-way ANOVA followed by Tukey's test, ns p > 0.05, **p < 0.01, ****p < 0.001, *****p < 0.0001. **D** Representative immunofluorescent images of 35-DIV forebrain organoids at 4-DPI with ΔNSs-LACV. White-dashed box indicates an inset. White arrows indicate IFIT1+ rosettes. Organoid sections were stained for LACV glycoprotein (*magenta*); IFIT1 (*green*); and DAPI (cell nuclei, *blue*). Scale bar of whole organoid—100 μm and *inset*—25 μm. Representative of 3 independent samples. Immunofluorescent images of ΔNSs-LACV-infected (**E**) or mock-treated (**F**) organoids. *White-dashed boxes* indicate *insets* labeled with corresponding numbers. *White arrows* indicate IFIT1+ rosettes. LACV glycoprotein (*magenta*); IFIT1 (*green*); Sox2 progenitor (*red*); cell nuclei, DAPI (*blue*). Scale bars of whole organoids—100 μm and inset—25 μm (N=three independent experiments)

response in human forebrain organoids. First, to determine whether the innate immune responses we observed were mediated through canonical IFN pathways, we used a janus-kinase (JAK) inhibitor, ruxolitinib, which blocks JAK1 and JAK2 downstream components of cytokine receptors, including IFN signaling. Specifically, we

infected 35-DIV forebrain organoids with Δ NSs-LACV for 24 h and sustained ruxolitinib treatment until 4-DPI for collection and immunofluorescence staining (Fig. 4A). JAK inhibition promoted viral antigen spread toward the center of the organoid, whereas intact JAK signaling during Δ NSs-LACV infection alone limited virus to the

periphery. Quantification of viral staining indicated significantly more Δ NSs-LACV signal dissemination with ruxolitinib treatment (Fig. 4B). This was further supported by quantitative RT-PCR for viral RNA (Fig. 4C). Moreover, inhibition of JAK signaling eliminated IFIT1 expression as determined by IF and quantitative RT-PCR (Fig. 4D, E), indicating a lack of bystander innate activation with ruxolitinib treatment. This reveals that intrinsic JAK-dependent neuronal responses are capable of limiting viral spread in forebrain organoids.

Next, to investigate if IFIT1 expression in bystanders was mediated by type I IFN, we treated forebrain organoids with recombinant IFNB to activate type I IFN independent of viral infection. IFIT1 expression was upregulated along the periphery; however, both SOX2 positive and negative neurons expressed IFIT1 (Fig. 4A), indicating that innate immune activation was no longer limited to progenitors. Treatment with recombinant IFNβ shows that both progenitors and non-progenitors have capacity for innate signaling. To see if this broad innate activation better restricted viral spread, we treated forebrain organoids with recombinant IFNβ throughout infection. Although we hypothesized a more robust IFN response with reduced viral burden, we observed virus localization and viral RNA levels similar to infection alone (Fig. 4A–C). Moreover, sustained IFNβ treatment throughout infection led to a similar induction of IFIT1 compared to infection alone (Fig. 4D, E). These data indicate that intercellular communication during viral infection sufficiently activates protective type I IFN pathways.

To directly evaluate the role of type I IFN in this intrinsic innate response, we next used CRISPR/Cas9 to knock-out the type I IFN receptor, *IFNAR1*, in iPSCs to generate IFNAR1–/– forebrain organoids (Supplemental Fig. 4). We infected 35-DIV IFNAR1–/– forebrain organoids with Δ NSs-LACV for 24 h and collected organoids

at 4-DPI for immunofluorescence and quantitative RT-PCR. We observed increased viral presence and an absence of IFIT1 protein (Fig. 4F). Moreover, quantitative RT-PCR revealed increased viral RNA (Fig. 4G) and diminished *IFIT1* expression (Fig. 4H), indicating a partial role for type I IFN signaling. Cumulatively, these data indicate that innate immune activation by bystander neural progenitors contribute to the antiviral response in human forebrain organoids. Specifically, neuronal communication between infected and bystander cells limit viral spread through type I IFN-dependent intercellular communication.

Spatial transcriptomics uncovers distinct regions of progenitor bystander activation

We leveraged spatial transcriptomics to investigate the interplay of bystander activation and protection during infection in forebrain organoids. Using the Visium platform, we obtained transcriptomes of 1409 spots in 8 Δ NSs-LACV-infected organoids and 1478 spots in 9 mock-treated organoids (Supplemental Figs. 5A and 5B). Each individual spot is 55 μ m and thereby contains several cells [22]. With the goal of understanding drivers of neuronal protection with respect to regions of viral infection, we aligned spatial data to LACV-stained organoids. We then conducted a clustering analysis that revealed seven distinct clusters (Fig. 5A, B). Each cluster represents different organoid regions that are all present in Δ NSs-LACV-infected and mock-treated conditions (Supplemental Fig. 5C).

We then aimed to evaluate differential levels of infection across the seven clusters. To quantitatively achieve this, we extracted spatially barcoded positions and integrated them with the corresponding immunofluorescence images (Fig. 5C, Supplemental Figs. 5A and 5B). Quantification of the mean fluorescence intensity

(See figure on next page.)

Fig. 4 Interferon signaling within bystander neural progenitors limits viral spread and replication. A-E 35-DIV forebrain organoids were infected with 2.5×10^6 PFU Δ NSs-LACV alone; 2.5×10^6 PFU Δ NSs-LACV and ruxolitinib (janus-kinase inhibitor); treated with recombinant IFN β alone; or 2.5 \times 10⁶ PFU Δ NSs-LACV and recombinant IFN β . Infection for 24-h followed by daily media changes and sustained ruxolitinib or recombinant IFNβ treatment until sample collection at 4-DPI for immunofluorescent staining or quantitative RT-PCR. A Representative immunofluorescent images. White-dashed boxes indicate insets. Sectioned organoids were stained with LACV glycoprotein (magenta); IFIT1 (green); and SOX2 progenitor (red). Scale bars of whole organoids—100 µm and insets—25 µm. B Quantification of LACV+ area relative to DAPI+ area in immunofluorescent images (A). C Fold change of LACV RNA at 4-DPI was determined by quantitative RT-PCR relative to housekeeping gene, HPRT. D Quantification of IFIT1 mean fluorescent intensity in immunofluorescent images (A). E Fold change of IFIT1 at 4-DPI as determined by quantitative RT-PCR relative to housekeeping gene, HPRT. 2-3 sections per experiment were used for quantification of immunofluorescent images. Data presented as means ± SEM (N=three independent experiments). Statistical analyses performed with one-way ANOVA followed by Tukey's test. ${\bf F}$ Representative immunofluorescent images of IFNAR1 knockout (IFNAR1 -/-) organoids that were mock-treated or infected with 2.5 × 10⁶ PFU ΔNSs-LACV for 24-h followed by daily media changes until 4-DPI. Sectioned organoids were stained with LACV glycoprotein (magenta) and IFIT1 (green). Scale bars of whole organoids—100 µm. G, H Wild type (+/+) or knock out (-/-) IFNAR1 forebrain organoids were infected with ΔNSs-LACV for 24-h followed by daily media changes until 4-DPI. Fold change of LACV RNA (G) and IFIT1 (H) was determined by quantitative RT-PCR relative to housekeeping gene, HPRT. Data presented as means ± SEM (N = five independent experiments). Statistical analysis performed with unpaired Student's t test, ns p > 0.05, *p < 0.05, **p < 0.01, ****p < 0.001, ****p < 0.001, ****p < 0.001

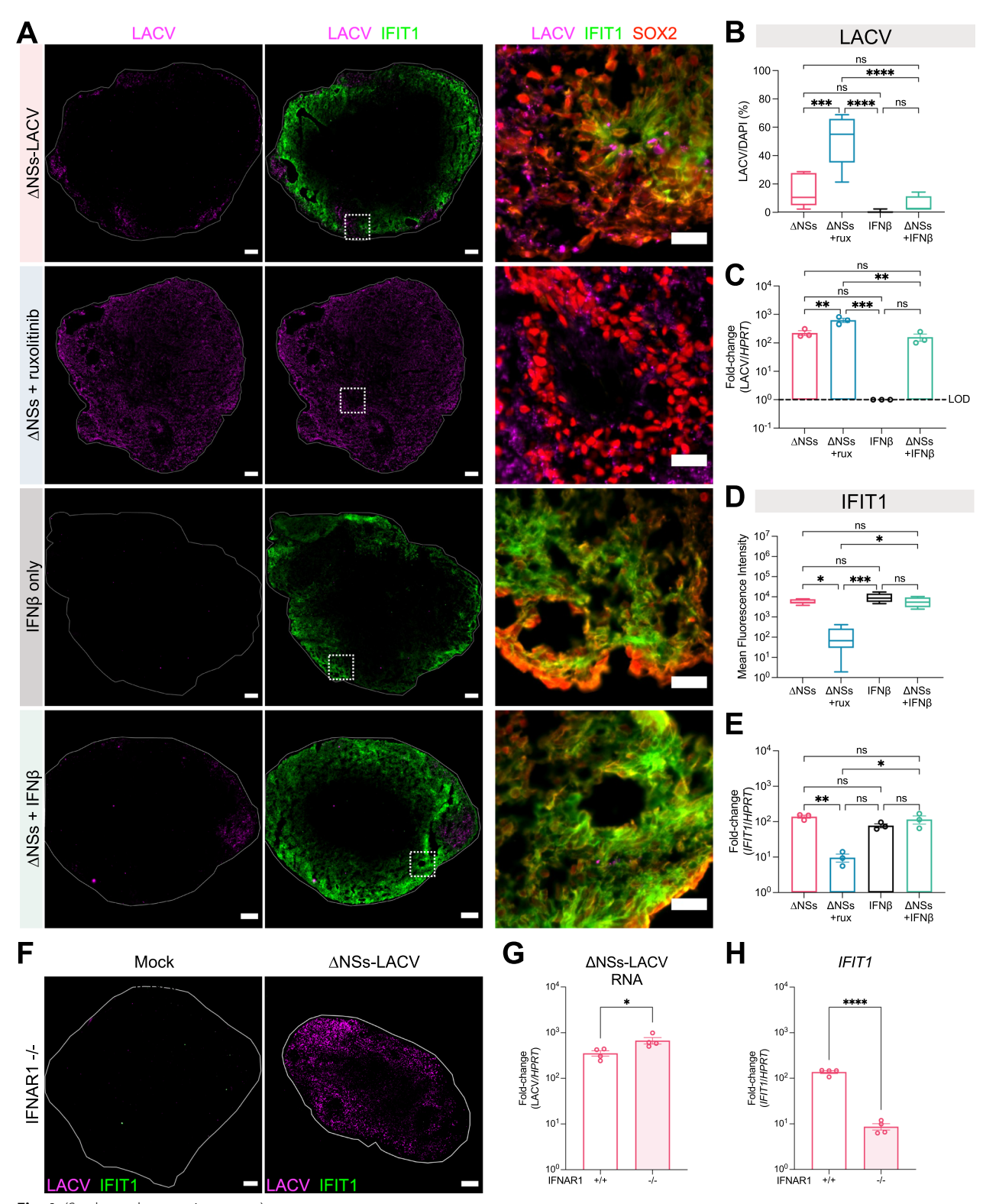


Fig. 4 (See legend on previous page.)

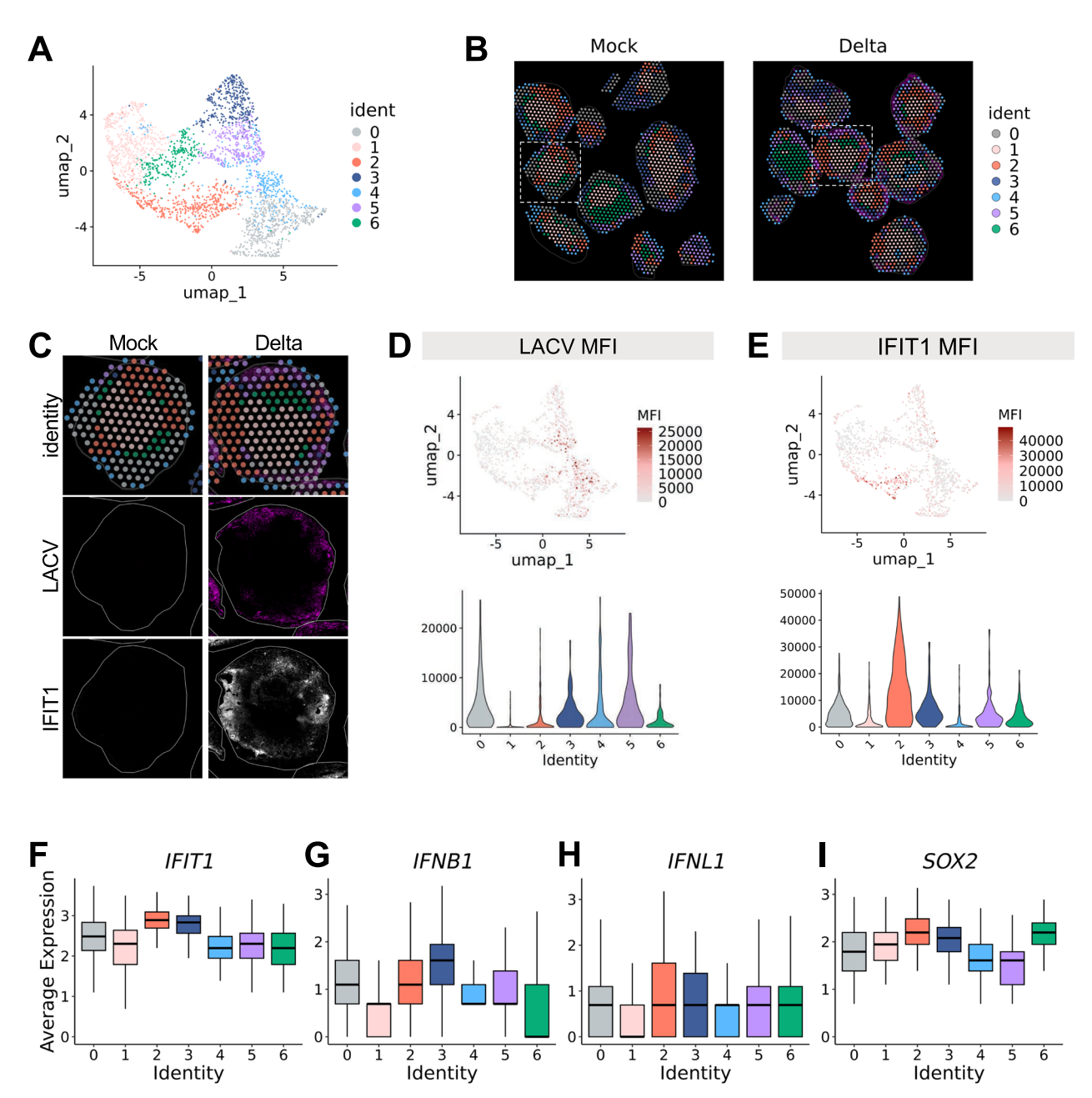


Fig. 5 Spatial transcriptomics uncovers distinct regions of progenitor bystander activation. 35-DIV forebrain organoids were mock-treated or infected with 2.5 × 10⁶ PFU ΔNSs-LACV and collected at 4-DPI for spatial transcriptomics using the Visium platform. **A** Uniform manifold approximation and projection (UMAP) of spatial transcriptomics spots that are representative of 1407 spots in 8 ΔNSs-LACV-infected organoids and 1470 spots in 9 mock-treated forebrain organoids. **B** Spatial clusters were aligned to immunofluorescent images of mock-treated or ΔNSs-LACV-infected samples. Serial sections were stained with LACV glycoprotein (*magenta*). **C** Representative organoids (*dashed-white boxes* in **B**) with spatial clusters (identity) and aligned immunofluorescent images below; Serial sections were stained with LACV glycoprotein (*magenta*) and IFIT1 (*white*). Quantification of LACV glycoprotein (**D**) or IFIT1 (**E**) mean fluorescence intensity (MFI) within each spot of ΔNSs-LACV-infected organoids using ImageJ. *Upper*, data represented in UMAP feature plot and *lower*, data represented as violin plot. Box plots showing *IFIT1* (**F**); *IFNB1* (**G**); *IFNL1* (**H**); and *SOX2* (**I**) expression in ΔNSs-LACV-infected organoids

(MFI) of LACV signal within each spot showed highly infected regions were represented by clusters 0, 3, 4 and 5 (Fig. 5D); areas that primarily mapped to the edges of

the organoids (Fig. 5C). However, clusters 1, 2 and 6 had little to no infection (Fig. 5D). Clusters 1 and 6 mapped primarily to the center of the organoids, where we do

not typically see viral spread, unless type I IFN signaling is compromised (Fig. 4A). Intriguingly, cluster 2 mapped along organoid edges, yet had little to no infection compared to other regions along the perimeter (Fig. 5B). This suggests that cluster 2 might represent regions of intercellular communication capable of protective immunity.

Next, to investigate if either of these regions represented bystander activation, we similarly quantified MFI for IFIT1 protein expression within each spot (Fig. 5C). Given the absence of IFIT1 signal in mock organoids, we focused further analysis on ΔNSs-LACV-infected organoids. We found that cluster 2 distinctly had the highest IFIT1 protein expression (Fig. 5E). However, gene expression data showed all clusters were positive for *IFIT1* transcripts, but clusters 2 and 3 had the highest expression (Fig. 5F). Given that we found bystander activation was type I IFN-dependent (Fig. 4), we evaluated gene expression of all type I IFNs and only identified IFNβ (*IFNB1*) as virally induced (Fig. 5G and Supplemental Fig. 5D). Interestingly, we also found similar expression levels of IFN1 (IFNL1), a type III IFN capable of inducing antiviral immunity, compared to IFNB1 (Fig. 5H). Although clusters 2 and 3 had similar gene expression, the lower LACV presence in cluster 2, despite proximity to LACVinfected regions, suggests that this cluster represents regions of bystander activation.

We previously noted that bystander activation was mediated by neuronal progenitors, thus, we sought to evaluate *SOX2* gene expression across clusters. We observed elevated *SOX2* expression in cluster 2; however other clusters also exhibited similar expression levels (Fig. 5I). This indicates that not all intercellular communication of progenitors ultimately results in protective bystander antiviral responses. Taken together, by combining protein and gene expression dynamics, we uncovered distinct regions of progenitor bystander intercellular communication that elicit neuron intrinsic protective antiviral immunity.

Spatial resolution reveals critical underpinnings of protective antiviral response in neurons

The identification of unique progenitor antiviral regions led us to further investigate the underlying mechanisms of protection following Δ NSs-LACV infection. Knowing cluster 2 had elevated IFIT1 expression and limited viral infection, we sought to identify clusters that lacked protection. Using the spot quantification of IFIT1 and LACV MFI (Fig. 5), we examined correlations between IFIT1 and LACV protein expression (Supplemental Fig. 6A). Similar to our earlier observation, cluster 2 demonstrates high IFIT1 protein expression and low LACV presence, further supporting its identity as a distinct region that can mount protective antiviral responses (Fig. 6A). This

stands in contrast to clusters 0, 4, and 5, which had lower IFIT1 protein expression and elevated LACV signal (Fig. 6A) and clusters 1, 3, and 6, which had low IFIT1 and LACV signal (Supplemental Fig. 6B).

Next, we aimed to define the gene signatures contributing to this protective antiviral response. We conducted differential gene expression analysis comparing cluster 2 with clusters 0, 4, and 5 from ΔNSs-LACV-infected samples, which revealed both anti-viral and regulatory IGSs (Fig. 6B). Some ISGs have roles in LACV-antagonism, such as MX1, AXL, IFITM3, BST2, and STAT1 [9, 23, 24]. We also identified several other ISGs in cluster 2 that had not been previously associated with LACV, including RSAD2, IFI16, and OAS1/2/3 [25]. Together, these ISGs have defined roles that limit different stages of the viral life cycle and promote IFN responses. Intriguingly, we also identified IFI35 and IFI44/L, which negatively regulate IFN responses [26-28]. Mock-treated forebrain organoids largely lacked ISG expression, with cluster 2 having slightly elevated expression, suggesting potential priming of these regions prior to infection (Supplemental Fig. 6C). Taken together, these data suggest cluster 2 can uniquely orchestrate antiviral responses through robust induction of specific anti-viral and regulatory ISGs.

Discussion

Neurons have long been considered passive targets during viral infection [5, 7, 13–16], thereby limiting exploration of innate immune activation between uninfected bystander and infected neurons. We designed this study to investigate the role of intercellular crosstalk in mediating intrinsic neuronal immunity and its contribution to protective antiviral responses. We found that in the absence of viral antagonism, neurons transcriptionally induce robust IFN signaling and can effectively signal to uninfected bystander neurons (Fig. 1). Yet, in two-dimensional cultures, this dynamic response did not restrict viral spread. Interestingly, this differed in the context of viral infection in three-dimensional forebrain organoids, where we observed protective capacity (Fig. 3). There are many underlying differences between our two-dimensional and three-dimensional models, such the access of viral particles to cellular surfaces or the composition of neuronal subtypes. Nonetheless, our findings underscore the importance of neuronal architecture and heterogeneity in facilitating intercellular communication to produce effective antiviral responses.

Previous work evaluating LACV infection in cerebral organoids found that committed neurons transcriptionally expressed fewer ISGs than neural progenitors [9]. Similarly, we observed the most robust induction of ISGs in neural progenitors, both transcriptionally and at the protein level. Importantly, forebrain organoids at

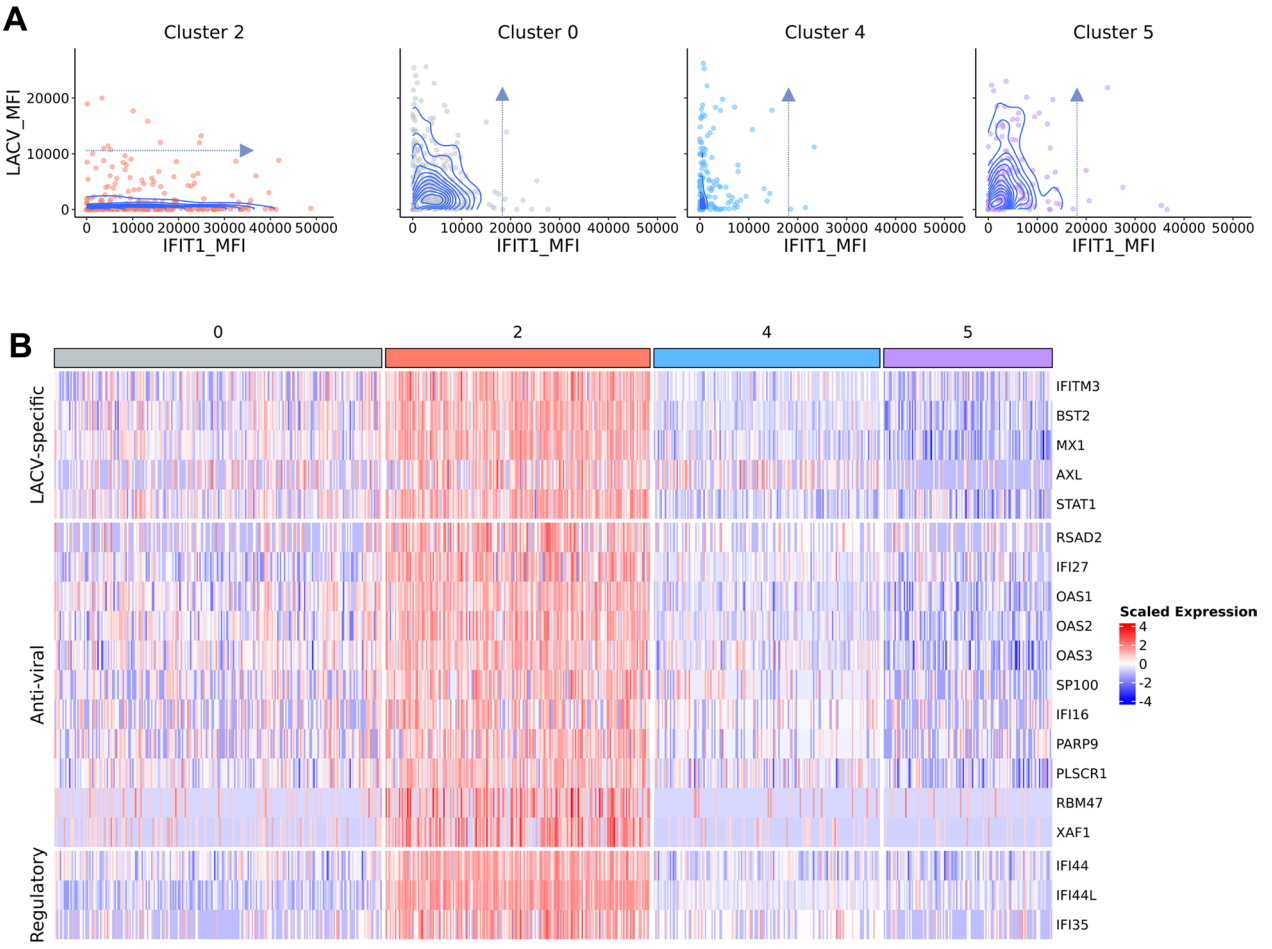


Fig. 6 Spatial resolution reveals critical underpinnings of protective antiviral response in neurons. 35-DIV forebrain organoids were mock-treated or infected with 2.5×10^6 PFU ΔNSs-LACV and collected at 4-DPI for spatial transcriptomics using the Visium platform (Fig. 5). Using Seurat, a subset of clusters 0, 2, 4, and 5 in ΔNSs-LACV-infected organoids were used for further analysis. **A** LACV glycoprotein or IFIT1 mean fluorescence intensity (MFI) within each spot of ΔNSs-LACV-infected organoids were quantified using ImageJ. Density plots represent correlation of LACV and IFIT1 MFI in clusters 0, 2, 4, and 5 of ΔNSs-LACV-infected organoids. Blue-dashed arrow indicates correlation trends. **B** Differential expression (DE) analysis comparing cluster 2 to clusters 0, 4, and 5 was conducted. 229 DE genes with a \log_2 fold-change >1 were identified. Interferon-stimulated genes and/or antiviral genes against LACV identified within the gene list were displayed in the heatmap display as scaled expression

this timepoint do not yet contain astrocytes [29], and therefore, cannot contribute to the observed immune responses. By considering location and infection status, we found that ISG-expressing neural progenitors were uninfected, bystander cells neighboring infected regions, indicating a previously unrecognized role in protection. Of note, we uncovered the capacity for bystander neural progenitors to prevent viral replication and spread. However, application of spatial transcriptomics revealed that not all neural progenitors were the same, and specifically, that regionality was important in antiviral signaling (Fig. 5). One limitation of our study is the resolution of spatial transcriptomics where each spot represents several cells. Thus, future studies should define gene expression changes at the

individual cell level in relation to the regional differences we observed.

Removal of viral antagonism enabled us to unmask the intrinsic capacity of neuronal innate immune activation and signaling. We demonstrated that type I IFN was a contributor to protective neuronal intrinsic responses with pharmacological inhibition and genetic knockout of IFN signaling (Fig. 4). Yet, our results do not rule out a role for other inflammatory responses. In fact, we observed greater viral replication control with ruxolitinib treatment, a janus-kinase inhibitor that broadly limits innate immune signaling, as compared to knockout of the type I IFN receptor alone. Interestingly, our spatial transcriptomics data uncovered the induction of a type III IFN, *IFNL1*, suggesting a potential role in protection

(Fig. 5). Future studies are needed to directly address the role of type III IFNs in neuronal intrinsic antiviral responses.

Our work has added to the field by defining gene signatures of protective neuronal intrinsic responses using differential gene expression analysis between protected and infected regions. Of note, we found that protected regions expressed distinct antiviral genes, including ISGs IFITM3 and BST2, which have known roles against Orthobunyaviruses [30, 31]. Given that LACV is an Orthobunyavirus, this suggests potential conserved mechanisms of protection within neurons. Similar to LACV, other orthobunyaviruses, including Bunyamwera and Schmallenberg viruses, contain IFN-response suppressing NSs proteins [32-35]. More broadly, neurotropic viruses contain numerous viral proteins that differentially antagonize innate immune signaling pathways in infected cells [12]. Future work should focus on determining the direct antiviral capacity of these ISGs in mediating protection against various neurotropic viruses and the interplay of this response with distinct immune evasion strategies.

Overall, by decoupling viral antagonism from neuronal immune signaling, our work reveals that intrinsic neuronal antiviral responses are intact within the context of cortical layers. Specifically, our work uncovers a previously unrecognized role for bystander neural progenitors in mediating signaling needed to orchestrate protective immunity amongst neurons. Further, we identify critical underpinnings of protection, including distinct antiviral genes. We envision that through defining underlying neuronal innate immune activation and signaling, we can leverage this foundational knowledge to inform development of novel antivirals to protect against neurotropic infection.

Materials and methods

Materials availability

Materials are available upon request from the lead author.

Mice

C57BL/6J mice (The Jackson Laboratory, Strain#000664) were maintained at the University of Pennsylvania under specific pathogen free conditions, on a 12-h light/dark cycle at 21 ±°1 °C, 50% humidity ±10%. All experiments were performed in adherence to the University of Pennsylvania's approved IACUC protocol.

Cell lines

Baby hamster kidney (BHK) (ATCC, Cat#CCL-10) and African green monkey kidney (Vero) (ATCC, Cat#CCL-81) cells were grown in Dulbecco's modification of eagle's medium (Corning, Cat#10-013-CV)

supplemented with 10% fetal bovine serum (Sigma-Aldrich, Cat#F2442), 1% penicillin–streptomycin (ThermoFisher Scientific, Cat#15140122), and 1% GlutaMAX (ThermoFisher Scientific, Cat#35050061). Human-induced pluripotent stem cell line C1-2 was kindly provided by Guo-Li Ming and maintained in mTSeR media (StemCell Technologies, Cat#100-1130) prior to fore-brain organoid generation protocol [36, 37]. All cell lines were routinely tested and found to be Mycoplasma-free at the Cell Center Services Facility (University of Pennsylvania).

Cortical neuron cultures

Embryos from embryonic day 16.5 of C57BL/6J mice (The Jackson Laboratory, Strain#000664) were dissected in cold 1× PBS. Cortices were resuspended and mechanically dissociated in room temperature Opti-MEM (Gibco, Cat#31985070) supplemented with 1% GlutaMAX. Cells were seeded on tissue culture treated plates coated with Poly-D-Lysine (Gibco, Cat#A3890401) according to manufacturer's recommendations. OptiMEM-GlutaMAX was replaced with neuronal media consisting of Neurobasal (Invitrogen, Cat#21103049) supplemented with 1% penicillin/streptomycin, 1% GlutaMAX and 2% B-27 (Gibco, Cat#17504044). After 4-days in-vitro (DIV), neuronal media was supplemented with 0.5uM cytosine beta-D-arabinofuranoside (Sigma, Cat#C1768). Neurons were cultured at 37 °C and 5% CO2 until 9-DIV where neuronal dendrites increased in number and branching.

Forebrain organoids

Forebrain organoids were generated using a previously described protocol [29, 36, 37]. Briefly, iPSCs were incubated at 5% CO₂, 37 °C and maintained until 60-85% confluent. iPSCs exhibiting signs of differentiations were excluded from organoid generation. Additionally, only iPSCs between passage numbers 15 and 45 were used in the study. At 0-DIV, iPSCs were seeded in low-attachment 96-well plates (Corning, Cat#3474) at a density of 50,000 to 200,000 cells/well in mTeSR1 supplemented with 10 µM of ROCK inhibitor (StemCell Technologies, Cat#72304). At 2-DIV, embryoid bodies (EB) were transferred using cut 1000uL pipette tips into 6-well plates in DMEM:F12 media (Gibco, Cat#11320033), supplemented with 20% Knockout Serum Replacement (Gibco, Cat#10828028), 1X GlutaMAX, 1X MEM Non-essential Amino Acids (Gibco, Cat#11140-050), 1X EmbryoMax 2-Mercaptoethanol (Sigma-Aldrich, Cat#ES-007-E), 1X Penicillin/Streptomycin, 1uM LDN193189 (Stem-Cell Technologies, Cat#72147), 1 mM SB-431542 (StemCell Technologies, Cat#72234) and 2 $\mu g/mL$ 0.2% heparin solution (StemCell Technologies, Cat#7980). Media changes were performed daily. At 6-DIV, EB

media was replaced with induction media consisting of DMEM:F12, 1X N-2 Supplement (ThermoFisher Scientific, Cat#17502048), 1X Penicillin/Streptomycin, 1X NEAA, 1X GlutaMAX, 1 μM CHIR99021 (StemCell Technologies, Cat#72054), and 1 µM SB-431542. Round EBs with bright edges were selected at 7-DIV, coated with Matrigel, and plated on ultra-low-attachment 6-well plates (Corning, Cat#3471). Media was changed every other day until 14-DIV when EB-Matrigel complexes were disassociated. EBs, now organoids, were maintained until 35-DIV with daily media changes consisting of 1:1 Neurobasal media and DMEM/F12 supplemented with 1X N-2, 1X B-27, 1X GlutaMAX, 1X MEM Non-essential Amino Acids, 1X EmbryoMax 2-Mercaptoethanol, 1X Penicillin/Streptomycin and 2.5 µg/mL of insulin (Sigma-Aldrich, Cat#I9278). All EBs and organoids were maintained at 5% CO₂, 37 °C and incubated on a shaking platform at 120 revolutions per minute, except when EBs were complexed with Matrigel.

iPSC IFNAR1 knockout using CRISPR/Cas9

Human IFNAR1 guide RNA (gRNA) targeting early exons were selected from previous literature (IFNAR1 gRNA: 5'-TAGATGACAACTTTATCCTG-3') gRNA and S. pyogenes Cas9 v2 were purchased from idtDNA (Cat#10007806). iPSCs displaying stem cell morphologies were selected to undergo electroporation. 300 ng of gRNA was incubated at room temperature with 7.5 mg of Cas9 for 10 min. Electroporation was then performed using Neon Electroporation Kit according to manufacturer's guidelines (ThermoFisher Scientific, Cat#MPK1025). Briefly, 1×10^6 iPSCs were resuspended in 5 mL of Resuspension Buffer R. 5 mL of resuspend cells was mixed and incubated with Cas9-gRNA complex. Using Neon pipette and tip, Cas9-gRNA was pulsed a single time into iPSCs at 1200 V for 30 ms. Cells were immediately transferred into 24-well plate (Corning, Cat#3524) coated with Matrigel and containing mTeSR1 supplemented with 10 mM ROCK inhibitor. Daily media changes were performed with mTeSR1 only until cells were 60% confluent and genomic DNA was extracted. IFNAR1 primers (Supplemental Table 1) targeting site of predicted gRNA-mediated Cas9 cut were designed and used to amplify region of interest. Amplicons were Sanger sequenced and clones with frameshift causing insertion/deletion mutations were maintained in culture. Clones underwent another round of subcloning to ensure single clonal population identity. These clones were again Sanger sequenced to confirm presence of frameshift causing deletion resulting in a premature stop codon in exon 2. The iPSC IFNAR1 knockout clone with no signs of differentiation was selected for validation and future experiments.

Virus stocks

Recombinant ΔNSs-La Crosse Virus (ΔNSs-LACV) with a point-mutation in the non-structural protein of the S segment [17]. (Kindly provided by Friedemann Weber, Jutus-Liebig University, Germany) and wildtype-La Crosse Virus (WT-LACV) (kindly provided by Sara Cherry) were propagated using the BHK cell line. For virus validation, RNA from infected BHK cells was reverse transcribed and a fragment of the LACV S segment was amplified by PCR as previously described [17]. EcoRI digestion of RT-PCR products was used to distinguish WT-LACV (two 572 and 217 bp fragments) from the recombinant ΔNSs-LACV (silent mutation lacking EcoRI digestion site). Tail digestion of the RT-PCR product was used to validate the point-mutation in recombinant ΔNSs-LACV (two fragments of 103 and 232 bp) from WT-LACV (no digestion site).

Virus infections

Murine cortical neurons were infected at 9-DIV by removing half of the media from cultures (neuron-conditioned media) and infecting the remaining volume at a multiplicity of infection (MOI) of 0.5 of WT- or ΔNSs-LACV at 37 °C. At 1-h post-infection (HPI), infectious media was removed, and cells were replenished with neuron-conditioned media for collection at 16-HPI, unless otherwise noted. Vero cells were infected with 5 MOI ΔNSs-LACV and collected using 0.05% trypsin (Gibco, Cat#25300054) at 16-HPI for fluorescence in situ hybridization (FISH) probe validation. Human-derived forebrain organoids were placed in 12-well tissue culture treated plates with two organoids per well at 35-DIV. Culture media was completely removed and replaced with fresh culture media containing 2.5×10^6 plaque forming units (PFU) of WT- or ΔNSs-LACV. Organoids were infected for 24 h at 37 °C and complete media changes occurred daily until 4-days post-infection (DPI).

Drugs and treatments

Human-derived forebrain organoids were infected with 2.5×10^6 plaque forming units (PFU) of WT- or Δ NSs-LACV supplemented with 20 uM ruxolitinib, a januskinase inhibitor (StemCell Technologies, Cat#73404) or 100 units/mL recombinant IFN β (PeproTech, Cat#300-02BC) where indicated at 37 °C for 24 h. After infection, virus containing media was removed and replaced with fresh media supplemented with 20uM ruxolitinib or 100 units/mL recombinant IFN β where indicated. Supplemented media changes were sustained until 4-DPI. To validate *IFNAR1* knockout in iPSCs and organoids, functional assays were performed on WT and IFNAR1 knockout iPSCs and 35-DIV forebrain organoids to determine response to IFN β stimulation. Specifically, confluent

iPSC cultures and forebrain organoids were treated with IFN β for 6 h prior to RNA extraction. Response to IFN β was assessed by measuring ISGs *IFIT1*, *OAS2*, and *MX1* using quantitative RT-PCR.

Neuron collection for flow cytometry

ΔNSs-LACV-infected and uninfected murine cortical neurons were collected at 16-HPI using an adapted previously described enzymatic and mechanical dissociation protocol [39]. Briefly, 9-DIV murine cortical neurons were washed with 1× PBS warmed to 37C. Neurons were then treated with a warmed dissociation buffer containing accutase (StemPro, Cat#A1110501), papain (Worthington Biochemical Corporation, Cat#LK003176), EDTA (Invitrogen, Cat#15575-038) and 1× PBS at 37 °C for 3-6 min until neuronal lifting was observed. Equal parts of neurobasal supplemented with 10% fetal bovine serum (Sigma-Aldrich, Cat#F2442) and 2 mM EDTA were added to neurons to neutralize the dissociation. Neurons were then transferred to a conical, mechanically dissociated using a 10 mL pipet and spun at 300×g at 4 °C for 4 min. Supernatant was removed and fresh 3.7% PFA (ThermoFisher Scientific, Cat#J19943-K2) was added for 10 min at room temperature. Equal parts of FISH buffer containing 1×PBS and 0.2 mg/mL RNase-free BSA (Sigma-Aldrich, Cat#B2518) was added and centrifuged at 300×g for 5 min at room temperature. Supernatant was removed and cells were resuspended in 500 µL 70% ethanol then transferred to a 1.5 mL Eppendorf.

Fluorescence in situ hybridization (FISH) staining and flow cytometry

Custom Stellaris® FISH Probes were designed against LACV M segment by utilizing the Stellaris® FISH Probe Designer (Biosearch Technologies, Inc.) available via Biosearch Technologies Stellaris designer resulting in 48 probes (Supplemental Table 2). Additionally, Stellaris® FISH Probes recognizing GAPDH or GFP (Biosearch Technologies, Inc., Cat#VSMF-3013-5 Cat#VSMF-1017-5) were used. Fixed murine cortical neurons and Vero cells were hybridized with the LACV M segment, GAPDH, or GFP FISH Probe sets labeled with CAL Fluor Red 610, following the manufacturer's instructions. Briefly, fixed cells were pelleted at 300×g for 5 min at room temperature and washed with wash buffer A (Biosearch Technologies, Inc., Cat#SMF-WA1-60). Cells were resuspended in hybridization buffer (Biosearch Technologies, Inc., Cat#SMF-HB1-10) containing the FISH Probe sets, then incubated in the dark at 37 °C for 30 min. Cells were then pelleted and resuspended in wash buffer A for 30 min at 37 °C. Cells were pelleted and incubated in wash buffer B (Biosearch Technologies, Inc., Cat#SMF-WB1-20) for 5 min at room temperature. Cells were then transferred to FACs tubes and washed with FISH buffer. Prior to flow cytometry, 1×DAPI was added to FISH probe-stained samples. All flow cytometry was conducted on the BD Biosciences LSRFortessa[™] Cell Analyzer. All FACs was conducted on the BD Biosciences Influx sorter.

RNA extraction, cDNA generation and quantitative RT-PCR

Cultured neurons or forebrain organoids were homogenized (MP Biomedical, Cat#116,004,500) in TRIzol (Invitrogen, Cat#15,596,018). RNA was extracted with Clean and Concentrator kit (Zymo, Cat#R1017) as per the manufacturer's instructions and RNA concentrations were measured with the ThermoFisher Scientific Nanodrop One spectrophotometer. cDNA was generated using 1 µg for neurons or 200 ng for forebrain organoids of RNA and iScript cDNA synthesis kit (Bio-Rad, Cat#1708890) as per the manufacturer's instructions. Quantitative RT-PCR was performed with Power SYBR Green Master Mix (ThermoFisher Scientific, Cat#4367659). Reactions were run via QuantStudio3 (50 °C: 2'; 95 °C: 10'; 40×95 °C: 15 s, 60 °C: 1') with the addition of a final melt curve (95 °C: 15 s; 60 °C: 1'; 95 °C: 1'). All samples were loaded in technical duplicates. Melt curves were confirmed for each sample, and no-template controls were run to ensure no contamination. Average Ct value was calculated per sample, which was normalized against housekeeping (hprt or HPRT) expression. Normalized expression was presented relative to the appropriate control.

Bulk RNA-sequencing

RNA was processed for bulk RNA-sequencing at the Children's Hospital of Philadelphia High Throughput Sequencing Core. All data was analyzed using an adapted form of the open-source DIY transcriptomics lecture materials [40].

Plaque assay

Infected supernatants from murine cortical neuron cultures or homogenates from forebrain organoids were serially diluted in DMEM (Corning, Cat#10-013-CV). Seeded BHK cells in a 6-well plate were treated with 200 μL of diluted supernatants and incubated for 1 h, with rotations every 15 min. Following incubation, inoculum was removed and replaced with MEM (Sigma-Aldrich, Cat#11430030) supplemented with 5% FBS, 1% GlutaMAX, 1% Non-essential amino acids, and 0.65% agarose (Lonza, Cat#50111). At 3-DPI, cells were fixed with 2 mL 10% NBF (ThermoFisher Scientific, Cat#22050105) and visualized using 0.1% crystal violet (ThermoFisher Scientific, Cat#C581-25). Plaques were manually counted to calculate virus titer.

Immunofluorescence

Primary murine neurons were washed with 1× PBS and fixed with 4% PFA for 15 min at room temperature. For sectioned human forebrain organoids, samples were incubated in 4% PFA for 30 min at room temperature, while rocking, and incubated in 30% sucrose overnight before being embedded in OCT (Sakura, Cat#4583) and cryosectioned (5–10 µm) using a Leica Cryostat. Wells and slides were washed three times with PBS prior to membrane disruption with PBS supplemented with Triton X (Sigma-Aldrich, Cat#T8787). Sample was blocked with PBS supplemented with 1% bovine serum albumin (Sigma-Aldrich, Cat#B2518) for 1 h prior to overnight incubation with primary antibodies (Rabbit monocolonal anti-Sox2, 1:100, CST, Cat#5067; Mouse anti-La Crosse Virus glycoprotein, 1:1000, This manuscript; Rabbit monocolonal anti-IFIT1, 1:100, CST, Cat#14769) diluted in blocking buffer. Samples were washed three times for 10 min with PBS supplement with 0.2% Tween20 (Biorad, Cat#1706531). After washing, samples were incubated for 1 h in secondary antibodies (Goat anti-mouse Cy3, 1:1000, Jackson ImmunoResearch, Cat#11-165-144; Goat anti-rabbit AF750, 1:500, Thermofisher Scientific, Cat#A21039) and 1xDAPI (ThermoFisher Scientific, Cat#AC202710100) diluted in blocking buffer. Following incubation, murine neuron samples were washed with PBST and imaged. Sectioned forebrain organoids were covered with mounting media and a coverslip was applied and sealed.

Spatial transcriptomics

Mock-treated or ΔNSs-LACV-infected were sectioned (10 mm) onto Visium CytAssist version 1 slides. Samples were stained with Eosin for processing with 10× CytAssist. Serial sections were stained with LACV glycoprotein targeting antibody, IFIT1 and DAPI for immunofluorescent imaging. Samples from CytAssist slides were processed for sequencing. Spatial data was aligned to LACV-stained organoids using 10X spaceranger. We next used Seurat to filter out spots with >5% mitochondrial genes, excluding a total of 10 spots. To evaluate organoid complexity, we applied a principal component cut-off of 15 and a clustering resolution of 0.4. All remaining analysis was conducted using Seurat.

Data analysis and availability

All sequencing data was analyzed using R Studio. Graphs were plotted and statistical analyses were performed using GraphPad Prism. Data are expressed as Mean \pm standard deviation (SD) or error of the mean (SEM). Number of biological samples used per experiment (n), number of individual experiments (N), and

statistical tests used for each experiment are included in figure legends. Statistical significance was determined by Unpaired Student's t tests for group means, One-Way or Two-Way ANOVA followed by post-Hoc multiple comparisons test as indicated. p < 0.05 was considered as significant. ns=non-significant, *p < 0.05, **p < 0.01, ****p < 0.001, ****p < 0.0001. Flow cytometry plots were generated using FlowJo. Immunofluorescence images were visualized using NIS-Elements and ImageJ.

Supplementary Information

The online version contains supplementary material available at https://doi.org/10.1186/s12974-025-03381-y.

Additional file 1: Supplemental Figure 1. Recombinant virus and FISH probe validation. (A-B) BHK cells infected with wild-type-La Crosse Virus . (WT-LACV) or recombinant ΔNSs-La Crosse Virus (ΔNSs-LACV) at 5 MOI, followed by RNA extraction at 16-hours post-infection (HPI). Lack of EcoRl digestion of ΔNSs-LACV demonstrates the silent mutation used to distinguish recombinant virus (A). Tail digestion validates ANSs-LACV's inability to express NSs due to the ablation of the reading-frame as in (B) (N = one independent experiment). (C) Vero cells and murine cortical neurons infected at 5 MOI and 0.5 MOI ΔNSs-LACV, respectively. Cells were collected for FISH staining at 16-HPI with probes targeting GAPDH (positive control), GFP (negative control) or LACV (M segment). Histograms represent cells analyzed using flow cytometry (N = one independent experiment). (D) Representative flow cytometry histograms with FACSsorted mock-treated neurons overlayed on ANSs-LACV-infected neurons collected at 16-HPI. LACV RNA was labeled with FISH probes (CAL Fluor Red 610) (N= two independent experiments). (E-F) Fold change of LACV RNA relative to housekeeping gene, Hprt, determined by quantitative RT-PCR (E) and virion production determined by plaque assay (F) kinetics following WT- or ANSs-LACV infection of murine cortical neurons at 1-, 16-, 24-, and 48-HPI. Neurons pooled from 1 litter per independent experiment. Data are presented as means \pm SEM (N = three independent experiments)

Additional file 2: Supplemental Figure 2. Radial organization and progenitor cells in forebrain organoids. (A) Model and brightfield images of 35-days in-vitro (DIV) human induced pluripotent stem cell-derived forebrain organoid generation. (B) Immunofluorescent images displaying neural progenitors that form neural rosettes in mock 35-DIV forebrain organoids. Organoid sections were stained with SOX2 (neural progenitor, red) and DAPI (cell nuclei, blue). Solid-white lines outline organoids and dotted-white lines outline neural rosettes based on DAPI and SOX2 staining. Scale bar of whole organoids – 100µm. (C) Immunofluorescent images displaying the viability of forebrain organoids and neuronal heterogeneity in mock 35-DIV forebrain organoids. Organoid sections were stained with SOX2 (neural progenitor, red); MAP2 (mature neurons, grey); and DAPI (cell nuclei, blue). Scale bar of whole organoids – 100µm.

Additional file 3: Supplemental Figure 3. Infection of forebrain organoids with LACV induces MX1 and OAS2. 35-days in-vitro (DIV) human induced pluripotent stem cell-derived forebrain organoids were infected with 2.5x106 PFU WT-LACV; Δ NSs-LACV; or mock treated for 24-hours. Organoid media was replenished with fresh media daily until sample collection at 4-days post-infection (DPI). (A) Fold change of MX1 and OAS2 was determined by quantitative RT-PCR relative to the housekeeping gene HPRT. Data are presented as means \pm SEM (N = four biological replicates). Statistical analysis performed with one-way ANOVA followed by Tukey's test, ns p>0.05, **p<0.01, ***p<0.001, *****p<0.0001.

Additional file 4: Supplemental Figure 4. IFNAR knockout forebrain organoids do not respond to IFN β stimulation. (A) Schematic of CRISPR/Cas9 guideRNA-mediated knockout of IFNAR1 gene. (B-D) Wild type (+/+) or knock out (-/-) IFNAR1 iPSCs treated with recombinant IFN β or mocktreated for 6 hours. Fold change of IFIT1 (B), OAS2 (C), and MX1 (D) RNA as determined by quantitative RT-PCR relative to the housekeeping gene

HPRT, normalized to mock. Data are presented as means \pm SEM (N = four independent experiments). Statistical analysis performed with two-way ANOVA followed by Tukey's test. (E) Representative brightfield images of IFNAR1 +/+ or -/- at 1-DIV embryoid bodies and 35-DIV forebrain organoids. (F) 35-DIV IFNAR1 WT and KO forebrain organoids treated with recombinant IFN β or mock-treated for 6 hours. Fold change of IFIT1 RNA as determined by quantitative RT-PCR relative to the housekeeping gene HPRT, normalized to mock. Data presented as means \pm SEM (N = five independent experiments). Statistical analysis performed with two-way ANOVA followed by Tukey's test, ns p>0.05, *p<0.05, **p<0.01

Additional file 5: Supplemental Figure 5. Spatial transcriptomics alignment and clustering reveal seven distinct clusters. (A-B) 35-DIV Mock-treated (A) or Δ NSs-LACV-infected (B) forebrain organoids with eosin staining aligned with fiducial markers; LACV glycoprotein (magenta) immunofluorescence staining aligned with 10x spatial spots; LACV glycoprotein (magenta) immunofluorescence images alone; and LACV glycoprotein (magenta) immunofluorescence images overlayed with Uniform manifold approximation and projection (UMAP) clustering of spatial transcriptomics spots. (C) UMAP clustering of spatial transcriptomics spots grouped by conditions, mock-treated or Δ NSs-LACV-infected. (D) Dot plot of FIFT1, IFNB1, IFNL1 normalized and variance-scaled gene expression, and percent spots expressing, grouped by conditions.

Additional file 6: Supplemental Figure 6. Extended analysis of spatial transcriptomics dataset from forebrain organoids. (A) Correlations of LACV and IFIT1 MFI for all spatial transcriptomics spots in Δ NSs-LACV-infected organoids quantified in Figure 5, grouped by clusters. (B) Density plots of clusters 1, 3, and 6 representing correlations of LACV and IFIT1 MFI in Δ NSs-LACV-infected organoids quantified in Figure 5. (C) Dot plot of interferon-stimulated genes normalized expression, and percent spots expressing. (D) Heatmap displaying 10883 differentially expressed (DE) genes identified through an unbiased DE analysis comparing clusters 0, 2, 4, and 5 to one another followed by a log2 fold-change greater than 1. Genes upregulated in cluster 2 were used for further analysis in figure 5D.

Additional file 7: Supplemental Table 1. Primer sequences used in this study.

Additional file 8: Supplemental Table 2. CAL Fluor Red 610 FISH probes targeting LACV M segment.

Additional file 9: Supplemental Table 3. Differentially expressed genes comparing clusters 0, 2, 4, and 5 from spatial transcriptomics dataset of Δ NSs-LACV-infected organoids.

Acknowledgements

We thank Dr. Friedemann Weber from the Jutus-Liebig University, Germany, for providing the recombinant ΔNSs-La Crosse virus; Dr. Sara Cherry from the University of Pennsylvania, Philadelphia, PA, USA, for La Crosse virus glycoprotein targeting antibodies; Molecular Pathology & Imaging Core (MPIC) from the University of Pennsylvania, Philadelphia, PA, USA, and 10x Genomics for assistance with spatial transcriptomics; Flow Cytometry Core facility at the University of Pennsylvania, Philadelphia, PA, USA, for sorting; Dr. Scott Sherrill-Mix from the University of Michigan for assistance with sequencing analysis.

Author contributions

S.G.N.: study conceptualization, study design, experimental work, data interpretation, RNA-seq data and bioinformatic analysis and manuscript writing. C.V.: study design, experimental work, manuscript review and editing. C.B.: study design, experimental work, manuscript review and editing. G.M.: study design, data interpretation, and manuscript review. K.A.J.: funding acquisition, study conceptualization, study design, manuscript writing, supervision.

Funding

This work was supported by the University of Pennsylvania Office of the President (KAJ), the University of Pennsylvania Office of the Provost (CV and SGN), the Burroughs Wellcome Fund (CV) and Laurie Breyer (KAJ, SGN).

Availability of data and materials

Sequencing data (BioProject: PRJNA1228059) will be deposited and publicly available as of the date of publication. All original code will be deposited at Zenodo (https://doi.org/10.5281/zenodo.14907845) and will be publicly available as of the date of publication. Microscopy, sequencing data, and any additional information required to reanalyze the data reported in this paper is available from the lead contact, Kellie A. Jurado (kellie.jurado@pennmedicine.upenn.edu), upon request.

Lead contact

Further information and requests for resources and reagents should be directed to and will be fulfilled by the lead contact, Kellie A. Jurado (kellie. jurado@pennmedicine.upenn.edu).

Declarations

Ethics approval and consent to participate

Not applicable.

Consent for publication

Not applicable.

Competing interests

The authors declare no competing interests.

Received: 7 November 2024 Accepted: 15 February 2025 Published online: 05 March 2025

References

- Ludlow M, et al. Neurotropic virus infections as the cause of immediate and delayed neuropathology. Acta Neuropathol (Berl). 2016;131:159–84.
- Klein RS, et al. Neuroinflammation during RNA viral infections. Annu Rev Immunol. 2019;37:73–95.
- Peltier DC, Simms A, Farmer JR, Miller DJ. Human neuronal cells possess functional cytoplasmic and TLR-mediated innate immune pathways influenced by phosphatidylinositol-3 kinase signaling. J Immunol. 2010;184:7010–21.
- Chakraborty S, Nazmi A, Dutta K, Basu A. Neurons under viral attack: victims or warriors? Neurochem Int. 2010;56:727–35.
- Delhaye S, et al. Neurons produce type I interferon during viral encephalitis. Proc Natl Acad Sci U S A. 2006;103:7835–40.
- Miller KD, Schnell MJ, Rall GF. Keeping it in check: chronic viral infection and antiviral immunity in the brain. Nat Rev Neurosci. 2016;17:766–76.
- Cho H, et al. Differential innate immune response programs in neuronal subtypes determine susceptibility to infection in the brain by positivestranded RNA viruses. Nat Med. 2013;19:458–64.
- Telikani Z, Monson EA, Hofer MJ, Helbig KJ. Antiviral response within different cell types of the CNS. Front Immunol. 2022;13:1044721.
- Winkler CW, et al. Neuronal maturation reduces the type I IFN response to orthobunyavirus infection and leads to increased apoptosis of human neurons. J Neuroinflammation. 2019;16:229.
- Blakqori G, et al. La Crosse bunyavirus nonstructural protein NSs serves to suppress the type I interferon system of mammalian hosts. J Virol. 2007;81:4991–9.
- 11. Verbruggen P, et al. Interferon antagonist NSs of La crosse virus triggers a DNA damage response-like degradation of transcribing RNA polymerase II. J Biol Chem. 2011;286:3681–92.
- Vazquez C, Jurado KA. Neurotropic RNA virus modulation of immune responses within the central nervous system. Int J Mol Sci. 2022;23:4018.
- Kreit M, et al. Inefficient type I interferon-mediated antiviral protection of primary mouse neurons is associated with the lack of apolipoprotein I9 expression. J Virol. 2014;88:3874–84.
- Lin C-C, Wu Y-J, Heimrich B, Schwemmle M. Absence of a robust innate immune response in rat neurons facilitates persistent infection of Borna disease virus in neuronal tissue. Cell Mol Life Sci CMLS. 2013;70:4399–410.

- Narayanan D, et al. Immature brain cortical neurons have low transcriptional competence to activate antiviral defences and control RNA virus infections. J Innate Immun. 2023;15:50–66.
- Sorgeloos F, Kreit M, Hermant P, Lardinois C, Michiels T. Antiviral type I and type III interferon responses in the central nervous system. Viruses. 2013;5:834–57.
- Blakqori G, Weber F. Efficient cDNA-based rescue of La Crosse bunyaviruses expressing or lacking the nonstructural protein NSs. J Virol. 2005;79:10420–8.
- Schoen A, Lau S, Verbruggen P, Weber F. Elongin C contributes to RNA polymerase II degradation by the interferon antagonist NSs of La crosse orthobunyavirus. J Virol. 2020;94:e02134-e2219.
- Krishnaswami SR, et al. Using single nuclei for RNA-seq to capture the transcriptome of postmortem neurons. Nat Protoc. 2016;11:499–524.
- Amamoto R, et al. Probe-Seq enables transcriptional profiling of specific cell types from heterogeneous tissue by RNA-based isolation. Elife. 2019:8:e51452.
- 21. Yang Q, Hong Y, Zhao T, Song H, Ming G. What makes organoids good models of human neurogenesis? Front Neurosci. 2022;16: 872794.
- Williams CG, Lee HJ, Asatsuma T, Vento-Tormo R, Haque A. An introduction to spatial transcriptomics for biomedical research. Genome Med. 2022:14:68.
- Varela M, et al. Sensitivity to BST-2 restriction correlates with Orthobunyavirus host range. Virology. 2017;509:121–30.
- Miner JJ, et al. The TAM receptor Mertk protects against neuroinvasive viral infection by maintaining blood-brain barrier integrity. Nat Med. 2015;21:1464–72
- 25. Schoggins JW, Rice CM. Interferon-stimulated genes and their antiviral effector functions. Curr Opin Virol. 2011;1:519–25.
- Das A, Dinh PX, Panda D, Pattnaik AK. Interferon-inducible protein IFI35 negatively regulates RIG-I antiviral signaling and supports vesicular stomatitis virus replication. J Virol. 2014;88:3103–13.
- Das A, Dinh PX, Pattnaik AK. Trim21 regulates Nmi-IFI35 complex-mediated inhibition of innate antiviral response. Virology. 2015;485:383–92.
- DeDiego ML, Martinez-Sobrido L, Topham DJ. Novel functions of IFI44L as a feedback regulator of host antiviral responses. J Virol. 2019;93:e01159-e1219.
- Vazquez C, et al. Antiviral immunity within neural stem cells distinguishes Enterovirus-D68 strain differences in forebrain organoids. J Neuroinflammation. 2024;21:288.
- Carlton-Smith C, Elliott RM. Viperin, MTAP44, and protein kinase R contribute to the interferon-induced inhibition of Bunyamwera Orthobunyavirus replication. J Virol. 2012;86:11548–57.
- 31. Schoggins JW, et al. Pan-viral specificity of IFN-induced genes reveals new roles for cGAS in innate immunity. Nature. 2014;505:691–5.
- 32. Thomas D, et al. Inhibition of RNA polymerase II phosphorylation by a viral interferon antagonist *. J Biol Chem. 2004;279:31471–7.
- Gouzil J, et al. Nonstructural protein NSs of Schmallenberg virus is targeted to the nucleolus and induces nucleolar disorganization. J Virol. 2016;91:e01263. https://doi.org/10.1128/jvi.01263-16.
- Barry G, et al. NSs protein of Schmallenberg virus counteracts the antiviral response of the cell by inhibiting its transcriptional machinery. J Gen Virol. 2014;95:1640–6.
- Léonard VHJ, Kohl A, Hart TJ, Elliott RM. Interaction of Bunyamwera Orthobunyavirus NSs protein with mediator protein MED8: a mechanism for inhibiting the interferon response. J Virol. 2006;80:9667–75.
- Chiang C-H, et al. Integration-free induced pluripotent stem cells derived from schizophrenia patients with a DISC1 mutation. Mol Psychiatry. 2011;16:358–60.
- 37. Lancaster MA, et al. Cerebral organoids model human brain development and microcephaly. Nature. 2013;501:373–9.
- Wang R, Yang JF, Senay TE, Liu W, You J. Characterization of the impact of merkel cell polyomavirus-induced interferon signaling on viral infection. J Virol. 2023;97:e0190722.
- 39. Jerber J, Haldane J, Steer J, Pearce D, Patel M. Dissociation of neuronal culture to single cells for scRNA-seq (10x genomics). 2020.
- Berry ASF, et al. An open-source toolkit to expand bioinformatics training in infectious diseases. MBio. 2021;12:121421–9. https://doi.org/10.1128/ mbio.01214-21.

Publisher's Note

Springer Nature remains neutral with regard to jurisdictional claims in published maps and institutional affiliations.